Rock strength and structural controls on fluvial erodibility: implications for drainage divide mobility in a collisional mountain belt

Jesse R. Zondervan*, Martin Stokes, Sarah J. Boulton, Matt W. Telfer, Anne E. Mather

School of Geography, Earth and Environmental Sciences, University of Plymouth, Plymouth, PL4 8AA, United Kingdom

Correspondence to: Jesse R. Zondervan (jesse.zondervan@plymouth.ac.uk)

Highlights

- We calculate rock strength, erodibility and drainage divide mobility in the High Atlas Mountains
- The weakest rock-type in the High Atlas is up to two orders of magnitude more erodible than the strongest
- In gently deformed horizontal strata of the sedimentary cover the drainage divide is mobile
- Faulted and folded metamorphic sedimentary bedrock coincide with a stable drainage divide
- Exhumation of crystalline basement forces the drainage divide into the centre of exposed basement

Abstract

Numerical model simulations and experiments have suggested that when migration of the main drainage divide occurs in a mountain belt, it can lead to the rearrangement of river catchments, rejuvenation of topography, and changes in erosion rates and sediment flux. We assess the progressive mobility of the drainage divide in three lithologically and structurally distinct groups of bedrock in the High Atlas (NW Africa). The geological age of bedrock and its associated tectonic architecture in the mountain belt increases from east to west in the study area, allowing us to track both variations in rock strength and structural configuration which influence drainage mobility during erosion through an exhuming mountain belt. Collection of field derived

measurements of rock strength using a Schmidt hammer and computer based extraction of river channel steepness permit estimations of contrasts in fluvial erodibilities of rock types. The resulting difference in fluvial erodibility between the weakest and the strongest lithological unit is up to two orders of magnitude. Evidence of geomorphic mobility of the drainage divide indicates that such a range in erodibilities in horizontal stratigraphy of the sedimentary cover may lead to changes in erosion rates as rivers erode through strata, leading to drainage divide migration. In contrast, we show that the faulted and folded metamorphic sedimentary rocks in the centre of the mountain belt coincide with a stable drainage divide. Finally, where the strong igneous rocks of the crystalline basement are exposed after erosion of the covering meta-sediments, there is a decrease in fluvial erodibility of up to a factor of three, where the drainage divide is mobile towards the centre of the exposed crystalline basement. The mobility of the drainage divide in response to erosion through rock-types and their structural configuration in a mountain belt has implications for the perception of autogenic dynamism of drainage networks and fluvial erosion in mountain belts, and the interpretation of the geomorphology and downstream stratigraphy.

Keywords: collisional mountain belt, drainage divide, rock strength, erodibility, High Atlas

6200 words (excl. highlights, abstract, tables, figure captions, author contributions, funding, refs)

1 Introduction

Collisional mountains form the erosional focus of the Earth's surface. The tectonic and climatic interpretation of topography and related depositional stratigraphy depends on the understanding of the dynamics of bedrock rivers eroding these source areas. The central drainage divide of an orogen is the topographic divide between river catchments draining either flank. Any movement of the drainage divide can result in the rearrangement of catchments, rejuvenation of topography, and changes in erosion rates and sediment flux (Bonnet, 2009; Giachetta et al., 2014). Bedrock erodibility is expected to play a significant role in drainage divide reorganisation since heterogeneous

exhumation of weak and strong substrates can enhance and suppress erosion respectively (Giachetta et al., 2014; Whipple et al., 2017; Gallen, 2018). This is especially the case in post-orogenic settings where erosion is dominant over crustal thickening (Gallen, 2018; Bernard et al., 2019). However, the magnitude of erodibility variation within a mountain belt, and the mobility of the drainage divide as rivers erode through its stratigraphy are still relatively unexplored.

Collisional orogens are characterised by bedrock rivers eroding through variable rock strength and tectonic architectures, such as very strong crystalline basement, deformed strong meta-sediments, and sedimentary cover composed of weak as well as stronger strata. Recent numerical modelling studies show the complexity of incision into horizontal or gently dipping strata of varying erodibility (Forte et al., 2016; Perne et al., 2017), and also suggest lithologically-induced dynamic erosion is expected to be less prevalent in tilted and /or faulted strata that have been highly deformed (Forte et al., 2016). The results of these models imply drainage mobility might be prevalent during incision in sedimentary cover but not in more deformed components of a collisional mountain belt. In a field study, Gallen (2018) modelled the erosion of a hard horizontal rock layer in the Appalachians. This model predicts that a geologically instantaneous capture of the Upper Tennessee River catchment by the Lower Tennessee River occurred at 9 Ma, which has led to a shift in the drainage divide and explains observed subsequent topographic rejuvenation in the landscape visible today. In the Pyrenees, Bernard et al. (2019) show the drainage divide follows the position of high-strength, high-elevation plutons in the crystalline basement in the centre of the belt, suggesting a direct lithological control on the position of the central drainage divide. These field studies demonstrate the drainage divide can be mobile in near-horizontal sedimentary stratigraphy of mountain belts, and is likely to move to the centre of highly resistant plutons as they get exhumed in the axis of a collisional mountain belt. However, both studies also demonstrate the challenge of documenting drainage mobility, which is often only recognisable in instantaneous capture events which leave pervasive topographic evidence. In addition, whist numerical simulation studies are instrumental in predicting long-term processes in geomorphology which are hard to derive from observations of modern day

78 landscapes alone, these involve simplifications and it is challenging to model the full complexity of
79 lithologies and structural geology of a collisional mountain belt. Furthermore, the fluvial erodibility
80 of rock, which depends on rock mass strength as well as jointing and weathering, is challenging to
81 measure quantitatively (Bursztyn et al., 2015) and consequently the range of erodibility inputs in
82 modelling studies vary widely (Roy et al., 2015; Forte et al., 2016; Yanites et al., 2017).

83 Consequently, while theory and numerical models predict a role for bedrock erodibility in driving
84 drainage divide mobility, where and when this is expected to occur in the evolution of mountain
85 belts remains unexplored. The challenges of measuring and characterising bedrock erodibility
86 (Bursztyn et al., 2015) and drainage divide dynamics in field settings (Willett et al., 2014; Forte and
87 Whipple, 2018) remain key problems. Addressing this challenge requires a dataset on rock erodibility
88 that is combined with topographic measures of drainage divide mobility in a mountain belt where
89 erosion is dominant over tectonic advection, and where rivers erode through a lithologically variable
90 landscape. In this study, we aim to derive data and present it in a form that is useful for both field
91 geologists and numerical modellers alike. We focus our study on the central High Atlas Mountains
92 (Fig. 1), where different stages of orogenic landscape evolution, from erosion through gently dipping
93 sedimentary cover to exhumed crystalline basement occur along the length of the main drainage
94 divide, forming a natural experiment. Furthermore, the continental inland setting, low weathering
95 rates associated with an arid climate and low rates of tectonic activity make this mountain range an
96 ideal setting to study erodibility-induced drainage divide mobility. In this study, we quantify the
97 magnitude of variation in erodibility between rock types by: (i) extracting the normalised steepness
98 of rock units from a digital elevation model and (ii) collecting mechanical measurements of rock
99 strength in the field; and (iii) we quantify the mobility of the drainage divide using topographic
100 metrics. Our measures of rock erodibility and stratigraphic orientation are then used to
101 quantitatively assess when and where a drainage divide will move in response to erodibility variation
102 in the evolution of a collisional mountain belt in which rivers erode first through sedimentary cover,
103 secondly through meta-sediments and finally through crystalline basement. Results from this study

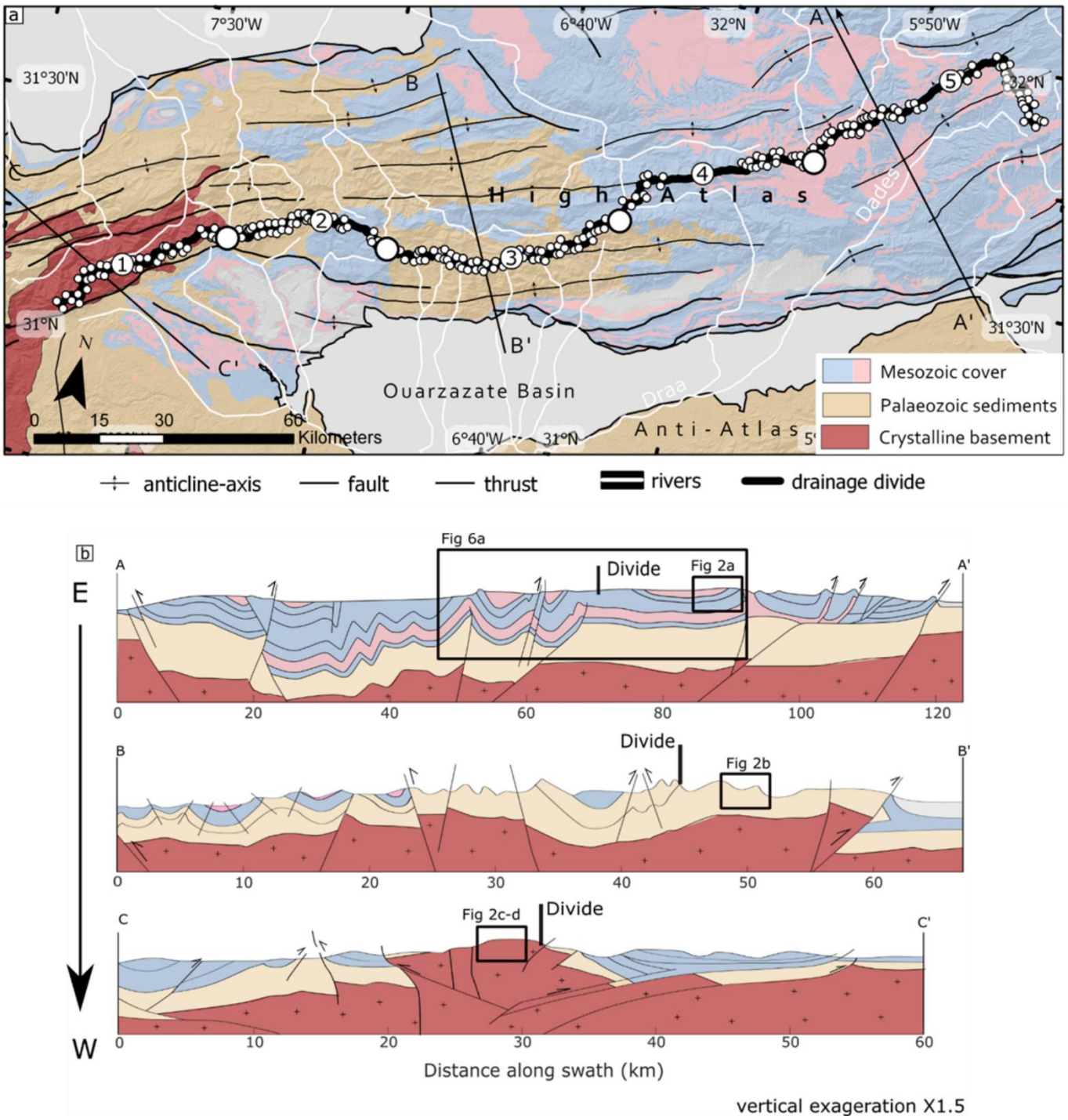

104

Figure 1 – a) Geological map of the central High Atlas, showing the distribution of Mesozoic sedimentary cover consisting of limestones (blue) and continental clastic sedimentary rocks (pink), Palaeozoic meta-sediments (orange) and crystalline basement (red). The chain is flanked by sedimentary basins: the Ouarzazate Basin to the south and the Haouz Basin to the North. Three cross-sections labelled A to C show the locations of cross-sections in b). Stream endpoint locations within 500 m of the drainage divide (headwaters) are marked as white dots. The drainage divide is marked on as a black line and is segmented into five equal lengths (Fig. 5). b) Cross-sections based on seismic sections modified from Errarhaoui (1998); Teixell et al. (2003). These cross-sections are vertically exaggerated by a factor of 1.5. The location of the drainage divide is marked on as black markers on the structural cross sections.

105 have implications for understanding long-term trends in the geomorphology and erosion of
106 mountain belts owing to the rock types and their structural configuration, and quantitatively
107 constrain the magnitude of contrasts in erodibility within a mountain belt which enables integration
108 of observation and modelling studies.

109 **2 Study area**

110 The study area is located in the centre of the High Atlas Mountains, focussed on the 250-300 km
111 length of the drainage divide bounded by the Ouarzazate Basin to the south and the Haouz Basin in
112 the north (Fig. 1). The drainage divide strikes along the structural grain of the mountain belt,
113 inherited by the configuration of a pre-existing rift (Babault et al., 2012). The age of exposed bedrock
114 and its associated tectonic architecture in the mountain belt increases from east to west in the study
115 area (Fig. 1). The along strike trends allow us to use location as a proxy for time in understanding the
116 mobility of the main drainage divide as river erosion exposes sedimentary cover to metamorphic
117 sedimentary rock, to crystalline basement. The sedimentary cover, older meta-sediments and
118 underlying crystalline basement have distinct lithologies with varying hardness and structural
119 weaknesses owing to the tectonic architecture of the mountain belt (Table 1). Thus, each
120 chronostratigraphic package has its own potential for drainage divide mobility which we investigate
121 in this study.

122 From east to west the drainage divide crosses first a landscape dominated by gently dipping beds of
123 Mesozoic carbonates and clastic sedimentary rock (Table 1) configured into low-amplitude long-
124 wavelength folds punctuated by spaced-out thrusts (Fig 1, Fig 2a) at an elevation of 2600 to 3000 m.
125 In this length of the divide, the Dades catchment lies to the south and incises into a long-wavelength
126 syncline exhibiting gently dipping strata, whereas directly north of the divide a concentration of
127 folding and thrusts offset strata dipping at higher angles to the surface (Fig. 1b). Next the drainage
128 divide decreases in elevation to ~2500 m, as it crosses a zone of dipping strata of faulted meta-
129 sediments (Table 1, Fig. 2b) in the centre of the study area (Fig.1). Finally in the west, the divide rises

Table 1 - chronostratigraphic packages labelled on Fig 1 with details of lithologies and structure

Chronostratigraphic package	Lithologies	Structure	Rock strength (see Table 2 for definitions)
Mesozoic sedimentary cover	massive marine platform limestones; continental red marls with gypsum; marine and continental conglomerates, sandstones, siltstones and micro-conglomerates	horizontal stratigraphy, gently deformed with spaced-out faults and thrust-top folds offsetting strata vertically	very weak – moderately strong
Palaeozoic meta-sediments	sandstones, shales, siltstones, schists	closely spaced faults, abundant jointing, steeply dipping and folded strata	moderately strong
Crystalline basement	granite, granodiorite, gabbro, dolerite, migmatite	massive outcrops of igneous rock, vertical or sheet fracturing in some outcrops	strong

back up to elevations > 2800 m as it runs over the edge of the exhumed crystalline basement consisting of igneous rocks with vertical or sub-vertical fracturing (Fig. 1, Table 1, Fig 2c-d).

The inland setting of the central High Atlas (800-1000 km from the coast) results in an absence of eustatic base level control on drainage development (Boulton et al., 2014). Furthermore, long-term 0.7-0.22 mm yr^{-1} uplift rates since 15 Ma derived from uplifted marine and lacustrine deposits (Babault et al., 2008), low incision rates (<0.2 mm yr^{-1}) of Quaternary river terraces generally lacking structural deformation (Stokes et al., 2017), and the low slip rate of 0.09-0.15 mm yr^{-1} for the most active neotectonic fault surveyed (Pastor et al., 2012), demonstrate both the absolute and differential rates of vertical motion are expected to be low in the High Atlas over the past 15 Ma to the present. Recorded glacial features related to Pleistocene glaciation establish that the snowline was at c. 3300 m in the High Atlas (Hughes et al., 2004). Since the main drainage divide varies in elevation between 2500-3000 m it has not been affected significantly by glacial activity. Thus, for our

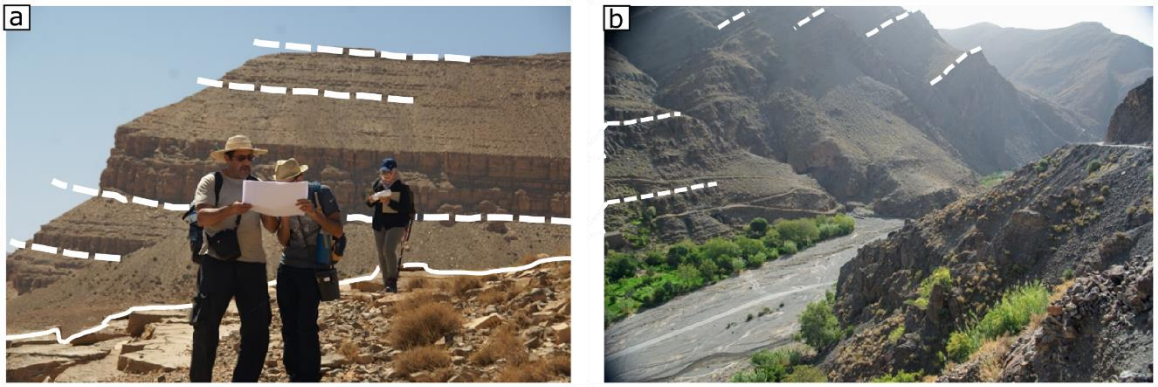

Figure 2 – field photos showing the lithologies and stratigraphic configuration of units within the three lithostratigraphic packages of the Atlas. a) In the Mesozoic weathering-resistant competent limestone beds dip at sub-horizontal angles. Within the interlayered limestones and weaker clastic rocks, variations in rock strength and weathering exist. b) In the Palaeozoic meta-sediments steeply dipping, sub-vertical strata are common. Road on the flood plain for scale. c) Massive crystalline basement exposed in is sometimes found jointed in vertical plains or d) as dome-shaped or massive igneous outcrops with vertical or sheet fracturing. House for scale at the bottom.

purposes the main control on the evolution of the High Atlas river network is the incision through the inherited tectonic architecture of lithological units and their contrasting strengths. Drainage development in the High Atlas is considered to be primarily the product of long-term uplift in the High Atlas following the exhumation of structurally distributed lithologies with different hardness, sometimes resulting in gorge formation (Stokes et al., 2008; Boulton et al., 2014), controlling where river terraces develop (Stokes et al., 2017) and affecting the connectivity of river channels and alluvial fans (Mather and Stokes, 2018). The High Atlas is set in a dry climate with low annual rainfall values less than a meter per year. The highest rainfall (775 mm) falls on the peaks, Toubkal in the west and Mgoun in the east, whilst the driest conditions are towards the Sahara desert in the southeast with annual rainfall of ~100mm (Fick and Hijmans, 2017). This means the effect of weathering on rock erodibility is expected to be low.

3 Methods

We measure two proxies of fluvial bedrock erodibility to constrain the contrast between lithological units. These data allow us to compare our field observations of drainage divide mobility with numerical models of river erosion through variable lithology. We systematically: 1) derive the normalised river channel steepness index from a digital elevation model (DEM) as a measure of a river channel's power to erode rock; 2) record compressive rock strength using a Schmidt hammer in the field as another measure of fluvial erodibility, and 3) extract topographic metrics of drainage divide mobility from the DEM along the length of the main drainage divide.

3.1 River profile analysis, rock type and fluvial erodibility

Rock type influences the river network by affecting the ability of rivers to erode into bedrock, determined by its fluvial erodibility. Numerical models that describe river erosion through bedrock often use the simple stream power law, in which the erosion rate at any particular point in a bedrock river channel is defined by:

$$E = KA^m S^n \quad \text{(Eq. 1)}$$

where *K* is an erodibility constant which depends on the rock-type over which the river channel flows as well as the climatic setting, *A* is local drainage area and *S* is local channel gradient, and *m* and *n* are constants that depend on basin hydrology, channel geometry, and erosion processes (Howard et al., 1994; Whipple and Tucker, 1999). Any change in the erodibility of rock type exposed will force the river to adjust its stream power by changing river channel slopes and thus can cause divide mobility as river networks respond. The use of this formula in field studies proves problematic because of the lack of data and robust methodology to determine the erodibility constant, *K*. However, equation 1 can be written as

$$S = \left(\frac{E}{K}\right)^{\frac{1}{n}} A^{-(m/n)} \quad \text{(Eq. 2)}$$

which may be recognised as a form of the empirical power law scaling local channel gradient (*S*) and drainage area (*A*):

$$S = k_{sn} A^{-\theta} \quad \text{(Eq. 3)}$$

$$k_{sn} = \left(\frac{E}{K}\right)^{\frac{1}{n}}$$

$$\theta = m/n$$

where *S* is the local channel slope (dimensionless), k_{sn} is normalised steepness index ($m^{2\theta}$) and θ is the concavity index (dimensionless). Calculations using the approach of Mudd et al. (2014) show that θ is ~ 0.45 for a range of catchments covering the extent of the drainage divide in the central High Atlas, which is the same value as used for the High Atlas by Boulton et al. (2014). This gives k_{sn} units of $m^{0.9}$. We assume that erosion is proportional to specific stream power, so that n = 1, and k_{sn} is inversely proportional to erodibility, *K*.

$$K \propto \frac{1}{k_{sn}} \quad \text{(Eq. 4)}$$

Unlike *K*, the k_{sn} of river channels can be readily determined from digital elevation models (DEMs) (e.g. Boulton et al., 2014; Gallen, 2018; Bernard et al., 2019). We therefore use k_{sn} as a measure of fluvial erodibility of geological units over which river channels flow in the High Atlas, provided that spatial variability in long term uplift is low, which is likely, for reasons outlined above (Section 2). Consequently, a factor of difference in k_{sn} between geological units will be an estimate of the factor of difference in their fluvial erodibility, *K*. We normalise k_{sn} values to the most erodible rock-type (see section 4.1), and then use Eq. 4 to convert these normalised average k_{sn} values to normalised *K* values. This enables a quantification of contrasts in erodibility *K* between rock-types in the High Atlas and their control on changes in river erosion rates and consequent mobility of the drainage divide.

We performed k_{sn} analysis using the Topographic Analysis Kit (Forte and Whipple, 2019), which produces a continuous k_{sn} grid. We use the ALOS Digital Elevation Model with a resolution of 30 m

200 from the Japan Aerospace Exploration Agency
201 (http://www.eorc.jaxa.jp/ALOS/en/aw3d30/index.htm) to perform the analysis. Boulton and Stokes
202 (2018) show that the ALOS DEM produces the most realistic river networks in the Moroccan High
203 Atlas and offers high resolution of geomorphic features. Finally, we extract the average and standard
204 deviation k_{sn} of each rock type using the digitised 1: 1 000 000 geological map of Morocco (Saadi et
205 al., 1985). Formations are grouped into lithological units that collectively comprise three groups:
206 Mesozoic sediments, Palaeozoic meta-sediments and crystalline basement over which the drainage
207 divide crosses from east to west (Fig. 1). For each of those packages we group lithological units
208 (Table 1): (i) gently folded massive marine platform limestone; (ii) interbedded red beds consisting of
209 mud and siltstone; (iii) interbedded sand-siltstones and conglomerates; (iv) folded and faulted meta-
210 sedimentary rocks such as schist and shale, and (v) faulted massive outcrops of igneous units. The
211 contrasts in k_{sn} of river channels flowing over rock-types includes the effects of both rock strength
212 and structural weaknesses on the resulting erodibility of bedrock.

213 *3.2 Mechanical rock strength measurements, rock type and erodibility*

214 A further approach to determine the fluvial erodibility of rock-types is measuring their mechanical
215 strength. The classic experiment by Sklar and Dietrich (2001) showed that erodibility of rock, *K*, in
216 the stream power law for bedrock river erosion is related to the inverse square of tensile strength
217 ($\sigma_\tau{}^2$). Thus, a measure of tensile strength and the difference between units enables the calculation
218 of contrasts in erodibility, *K*:

219 $$K \propto \frac{1}{\sigma_\tau{}^2} \qquad \text{(Eq. 5)}$$

220 However, measurements of tensile strength cannot be achieved easily in the field, and the most
221 commonly applied method of rock strength assessment in geomorphology is the Schmidt hammer
222 because of its portability (Goudie, 2006). The Schmidt hammer records the rebound velocity of a
223 plunger that strikes the rock surface and uses a range from 10 – 100. With the Schmidt hammer,

measurements of *in situ* uniaxial compressive rock strength in the landscape can be taken in large quantities, making it a very versatile instrument in landscape studies. The higher the rebound value, the higher the elastic strength of the rock, which is a measure of the uniaxial compressive strength (UCS) of a rock. Tensile strength (TS) represents the resistance to sediment impacts on the riverbed and its use has been advocated based on the stronger correlation of fluvial metrics with tensile strength than compressive strength (Bursztyn et al., 2015). But since compressive and tensile strength are correlated (UCS ~ 10*TS; Kahraman et al., 2012; Nazir et al., 2013), *K* is effectively also proportional to the inverse square of UCS:

$$UCS \propto \sigma_\tau \qquad \text{(Eq. 6)}$$

$$K \propto \frac{1}{UCS^2} \qquad \text{(Eq. 7)}$$

Thus, similar to the approach in 3.1, we normalise UCS values to the most erodible rock-type, and then use Eq. 7 to convert these normalised average UCS values to normalised *K* values. To produce a map of rock strength we digitised the 1:1 000 000 geological map of Morocco (Saadi et al., 1985) for the study area and assigned an average rock rebound value to each stratigraphic unit. Typically, ten to twenty Schmidt hammer measurements were taken at each location, totalling 690 readings throughout the central High Atlas with up to 132 readings per geological unit. Where rock strength measurements for geological units from field measurements were absent, we supplemented this with an existing database of Schmidt rebound values for lithological units reported from around the world (Goudie, 2006). This database contains Schmidt rebound measurements for 111 lithological units, in mostly arid environments similar to the High Atlas. For each stratigraphic unit without field measurements the average of values reported in the literature for the lithology of that unit is used. Units are combined in the same lithological groups as the k_{sn} data. The standard deviation of Schmidt hammer measurements and the range of values reported in the literature reflect the variation of rock strengths within the lithological units. Mean and standard deviation of Schmidt hammer rebound values (SHV) are then converted to UCS using the conversion which was derived by Katz et

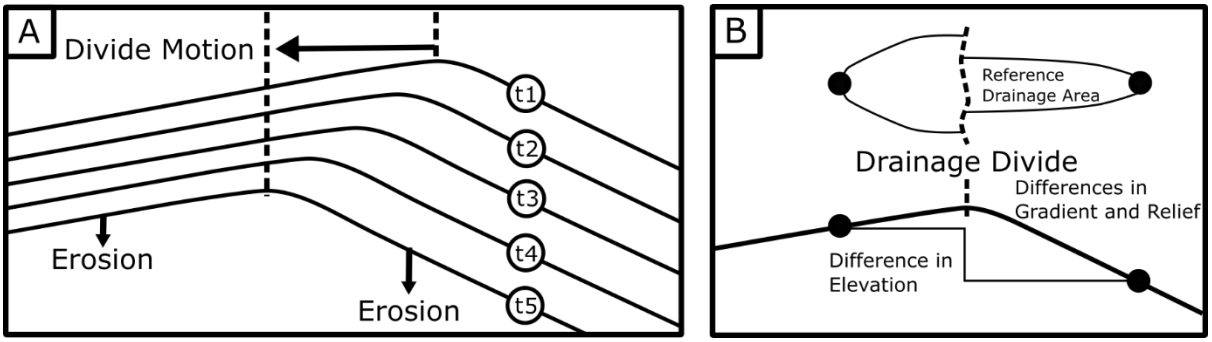

Figure 3 – principles of the Gilbert metrics for drainage divide stability, modified after Forte and Whipple (2018). Where channels are steeper on one side of the divide compared to the other, divide motion will be in the direction of low gradients where erosion is lower. B) Similarly, erosion will progress towards those channels with higher elevation channel heads.

al. (2000) ($UCS = 2.21e^{(0.07SHV)}$) for a range of carbonate rocks, sandstone, marble and igneous rocks with UCS values similar to those found in the study area. In contrast to the k_{sn} approach, the UCS of lithological units only takes into account the internal rock mass strength of bedrock, and thus does not account for structural weaknesses imposed by discontinuities such as bedding or jointing. Consequently, estimating variation in erodibility between rock-types using this approach may be expected to overestimate the erodibility of folded and faulted shales and schists and jointed igneous rock (Table 1).

3.3 Topographic analysis of the drainage divide

To determine the mobility of the drainage divide in response to erodibility variation and its structural configuration, we perform topographic analysis of the main drainage divide along the study length. The mobility and potential direction of movement of the drainage divide depends on erosion rates either side. Forte and Whipple (2018) coined the term Gilbert Metrics, named after Gilbert (1877) who first defined the law of unequal declivities. This law assumes that where divides are bounded by different channel gradients either side they are mobile, with higher erosion rates on the steeper sides leading to migration towards the side with lower channel gradients (Fig. 3). The topographic proxies for erosion rates across divides defined by Forte and Whipple (2018) are differences in headwater channel elevation, local headwater hillslope gradient and local headwater relief, which have proven useful for interpreting the relative mobility of catchment divides (Forte

and Whipple, 2018; He et al., 2019; Wang et al., 2019). Headwater channel elevation, local headwater hillslope gradient and local headwater relief were extracted from the ALOS DEM using methods outlined in Forte and Whipple (2018), at a reference drainage area 1 km^2. This drainage area is the critical threshold area upstream of which debris-flow-dominated colluvial channels are expected to dominate over stream-flow-dominated fluvial channels (Wobus et al., 2006). In a numerical landscape evolution model, Forte and Whipple (2018) test the applicability of the Gilbert metrics in a setting with erodibility contrasts across a drainage divide, and conclude that divide migration rate approximates a linear relationship with cross-divide differences in erosion rates and all three Gilbert metrics. To assess the mobility of the drainage divide we define five equal lengths of about 50 km each (Fig. 1), and in each the mean, standard deviation, standard error and bootstrap confidence interval of channel head values are calculated either side of the drainage divide.

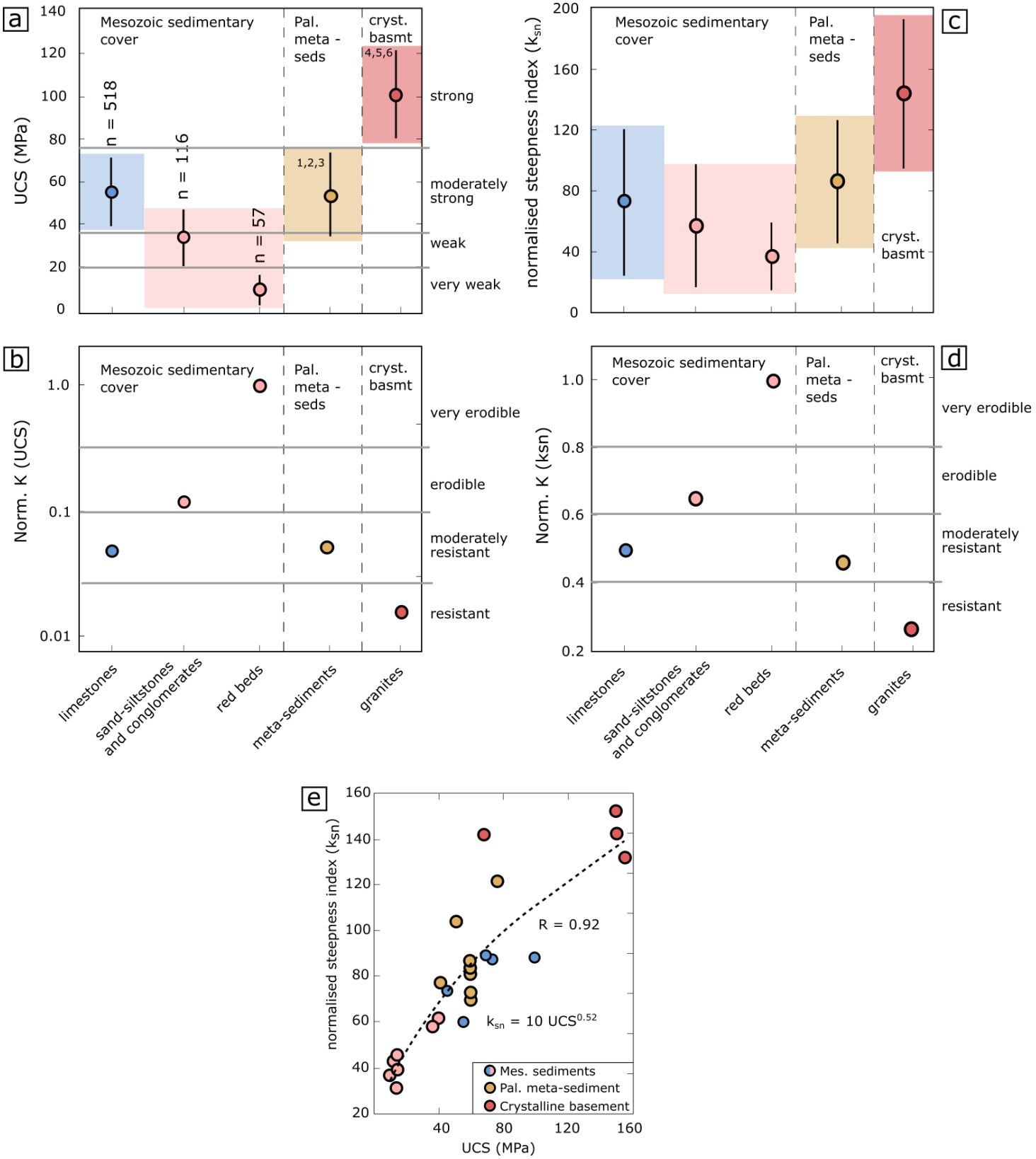

Figure 4 – Average and standard deviation of a) uniaxial compressive strength b) k_{sn} for every chronolithological unit. The number of values analysed for each lithology is displayed above the plots. Colours in graphs are in accordance with Fig. 1. Sources of compressive strength data: 1) Gokceoglu and Aksoy (2000) 2) Goudie (2006) &references cited therein 3) Goktan and Gunes (2005) 4) Karakus et al. (2005) 5) Pye et al. (1986) 6) Kahraman et al. (2002). Fluvial erodibility K for each chronolithological unit normalised against the weakest rock type derived from relative UCS values (c) and relative k_{sn} values (d). e) Power relationship between mean values of k_{sn} and UCS for every geological unit (geological map 1:100 000) coloured by chronolithological membership. R is the correlation coefficient. Classification of rock strength is based on Schmidt hammer values and other measures of rock strength summarised in Table 2, modified from Goudie (2006). Erodibility classification is based on rock strength (Table 2), and values of boundaries between classes vary with the approach to estimating normalised erodibility.

Table 2 – Classification of rock-type, strength and fluvial erodibility

Description	**Schmidt hammer value**	**Uniaxial Compressive strength**	**Characteristic rocks**	**Fluvial erodibility**
Very weak rock – crumbles under sharp blows with geological pick point, can be cut with pocket knife	10-30	1-20	Weathered and weakly compacted sedimentary rocks – rock salt, marls	Very erodible
Weak rock – shallow cuts or scraping with pocket knife with difficulty, pick point indents deeply with firm blow	30-40	20-35	Weakly cemented sedimentary rocks – siltstones and conglomerates	Erodible
Moderately strong rock – knife cannot be used to scrape or peel surface, shallow indentation under firm blow from pick point	40-50	35-75	Competent sedimentary rocks – limestone, dolomite, sandstone, shale, slate, schist	Moderately resistant
Strong rock – hand-held sample breaks with one firm blow from hammer end of geological pick	> 50	> 75	Competent igneous and metamorphic rocks – granite, migmatite, granodiorite, basalt	Resistant

Rock strength classification and descriptions modified from Table 2 in Goudie (2006)

4 Results

In plan view (Fig 1a), the drainage divide follows a sinuous form, with lengths mostly configured to ENE-WSW and WNW-ESE orientations. The divide tends to occupy northerly positions apart from a notable southerly segment in its central area. Only in the eastern end is there a marked deviation in divide orientation where a small length (20 km) changes to NW-SE.

With respect to erodibility, the drainage divide from east to west runs over bedrock of differing erodibilities, quantified through k_{sn} and UCS measurements.

4.1 K_{sn} and fluvial erodibility

From east to west, the drainage divide runs over moderately resistant to erodible and very erodible sedimentary cover, moderately resistant meta-sediments, and resistant crystalline basement (Fig. 1).

Red beds, other clastic sediments and limestones in the Mesozoic cover have mean k_{sn} values of 37, 59 and 74 $m^{0.9}$ with standard deviations of 25, 42 and 49 $m^{0.9}$ respectively (Fig. 4c). Palaeozoic meta-sediments average at 85 $m^{0.9}$ with a standard deviation of 41 $m^{0.9}$, whilst the crystalline basement has the highest k_{sn} at 146 with a standard deviation of 52 $m^{0.9}$ (Fig. 4c). Fluvial erodibility *K* values based on Eq. 4 and k_{sn}, normalised to the Mesozoic red beds (the weakest lithology: section 3.2), vary by a factor of four (Fig. 4d). The normalised *K* value for red beds is 1.0, with other clastics and limestone in the Mesozoic cover at 0.63 and 0.5 respectively. Normalised *K* for Palaeozoic meta-sediments is 0.44 whilst crystalline basement has the lowest normalised *K* at 0.26, about four times less erodible than the Mesozoic red beds. Categories of erodibility suggested based on the lithological grouping into rock strengths (Table 2) and their respective normalised *K* based on k_{sn} values are defined in Fig. 4d.

4.1 UCS and fluvial erodibility

Similar to the k_{sn} of rock units, the fluvial erodibility of bedrock along the length of the drainage divide based on UCS varies from alternating very erodible to moderately resistant rock in the sedimentary cover, to moderately resistant in the meta-sediments and resistant in the crystalline basement. The Mesozoic sedimentary cover has the largest range in UCS of the three chronostratigraphic packages, with red beds, other clastic sediments and limestones averaging 12, 36 and 57 MPa respectively, with standard deviations of 7, 12 and 18 MPa (Fig. 4a). UCS values for the Palaeozoic meta-sediment averages at 55 MPa with a standard deviation of 19 MPa, similar to the Mesozoic limestones (Fig. 4a). The igneous rocks of the crystalline basement have the highest UCS values with a mean and standard deviation of 101 and 20 MPa. Grouping of rocks into five classes is based on a table from Goudie (2006) which is based on Schmidt hammer values and other measures of rock strength (Table 2), and classes are marked on the UCS graph (Fig. 4a). Fluvial erodibility *K* values based on Eq. 7 and UCS, normalised to the weakest unit, vary by two orders of magnitude (Fig. 4b). The normalised *K* value for red beds is 1.0, with other clastic and limestone in

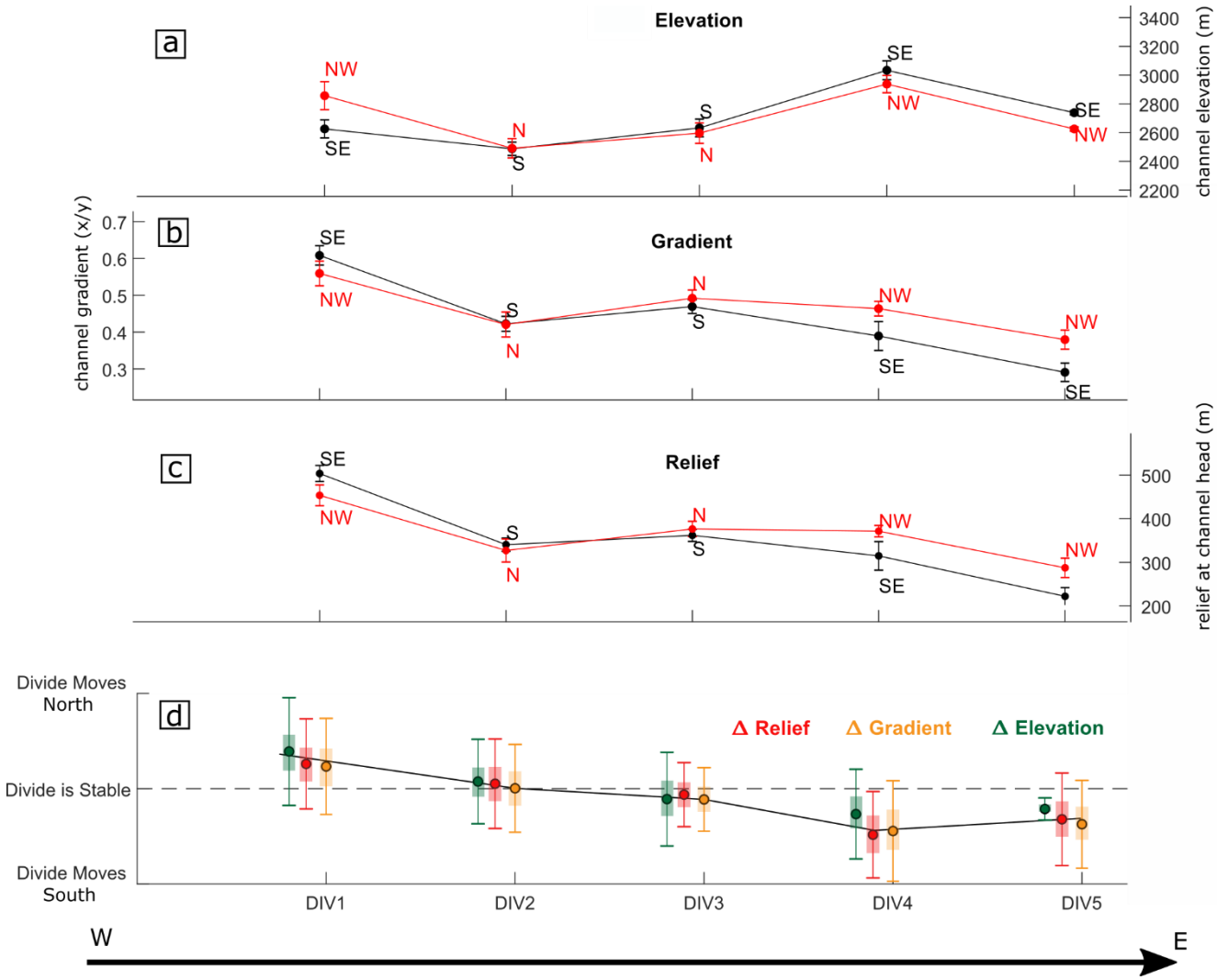

Figure 5 – Gilbert metrics for each length of the drainage divide (Fig. 1) from west to east. a-c) channel head mean and standard error elevation, gradient and relief respectively. d) Potential direction of divide migration indicated by the direction of mobility of the divide from the Gilbert metrics. Values are standardized to show the direction of mobility. Bars show the standard deviation and shaded boxes show bootstrap confidence intervals.

the Mesozoic cover at 0.1 and 0.05 respectively. Normalised *K* for Palaeozoic meta-sediments is 0.05 whilst crystalline basement has the lowest normalised *K* at 0.015, about two orders of magnitude less erodible than the Mesozoic red beds. Categories of erodibility suggested based on the lithological grouping into rock strengths (Table 2) and their respective normalised *K* values based on UCS are defined in Fig. 4c.

4.2 Drainage divide mobility

Normalised cross-divide delta values of the Gilbert metrics following Forte and Whipple (2018) show the magnitude and direction of mobility varies along the divide and that the divide is stable in the

central length of the divide (Fig. 5). Elevation of the drainage divide is high in both the east and west, around 2600-3000 m in DIV 1 and DIV 4-5, and lowest in the middle length at ~ 2500 m (Fig. 5a). This low elevation length (DIV 2-3) of the divide in the centre of the study area has equal headwater hillslope gradients and relief on both sides of the divide (Fig. 5b-c) suggesting a stable drainage divide in the meta-sedimentary rocks (Fig. 1, 5d). From west to east, headwater hillslope gradients and relief decrease from 0.6 (35°) and 500 m in in the crystalline basement of DIV 1 to 0.3 (15°) and 220 m in the Mesozoic sedimentary cover of DIV 5. Values of channel head elevation, hillslope gradient and relief differ either side of the drainage divide in the eastern (DIV 1) and western (DIV 4-5) lengths (Fig 5b-c). In DIV 1, the Gilbert metrics indicate northward movement of the divide (Fig. 5d) towards the centre of the exposed crystalline basement. This mobility is based on headwater values which are on average 169 m higher in elevation to the north, with lower hillslope gradients and relief, which differ by 0.06 (3.4°) and 50 m of relief (10%) across the divide (Fig. 5a-c). In DIV 4 and 5 in the Mesozoic cover the divide is significantly mobile towards the south (Fig. 5d), with channel head elevation contrasts of 96-113 m, a difference in hillslope gradients of 0.07-0.09 (4-5°) and relief 44-55 m (14-30%) (Fig. 5a-c).

5 Discussion

5.1 Rock strength, k_{sn} and fluvial erodibility

The theory and empirical relationships outlined in sections 3.1 - 3.2 predict that fluvial erodibility, *K* relates to UCS and k_{sn} in an inverse square (Eq. 7) and inverse relationship (Eq. 4), respectively. Thus, k_{sn} and UCS are expected to scale according to a square relationship. Instead, we find a square root relationship between k_{sn} and UCS (Fig. 4e). This suggests that either, Eq. 7 overestimates the effect of rock mass strength on the erodibility of rocks, or Eq. 4 underestimates the effect of lithology on river erosion. Most likely both of these statements are true. UCS does not explicitly include other factors influencing bedrock erodibility including the degree of weathering and structural discontinuities (Table 1), which especially through zones of deformation, will lead to more rapid

349 erosion of even hard rocks (high UCS) by fluvial systems. For example, Anton et al. (2015) and
350 Baynes et al. (2015) showed that canyons can be created by extreme flood events in basalt and
351 granite respectively, where the presence of discontinuities enables rapid erosion through fluvial
352 plucking and block topple. On the other hand, whilst the simple stream power model of bedrock
353 river erosion only accounts for changes in river channel slope, field studies show that rock strength
354 correlates with channel width (Allen et al., 2013), as well as valley width (Schanz and Montgomery,
355 2016) and can influence the efficiency of river bed load in eroding underlying bedrock (Brocard and
356 van der Beek, 2006). Based on the lithological effects on river channel and valley morphology
357 demonstrated by these field studies, using k_{sn} as a measure of rock erodibility in the stream power
358 model of bedrock river incision likely underestimates the effect of lithology on river erosion.
359 Effectively, the normalised *K* calculated using the k_{sn} and UCS approach give a lower and upper
360 bound of the contrast in erodibility *K* between rock types in the Atlas.

361 Thus, calculated through UCS measurements, *K* is expected to vary by two orders of magnitude (Fig.
362 4c), whereas if using the k_{sn}, *K* is expected to vary by a factor of four only (Fig. 4d). Whilst the
363 difference in values between these two approaches may appear large, the lack of constraints of *K* in
364 natural settings have led to numerical modelling studies varying widely in the range of erodibilities,
365 using from one (Forte et al., 2016), two (Yanites et al., 2017), to three orders of magnitude
366 difference between rock-types (Roy et al., 2015). Such a range of inputs is often based on the
367 experimental relationship between intact rock strength and erosion in the classic abrasion mill
368 experiment done by Sklar and Dietrich (2001), and the five orders of magnitude difference in *K*
369 derived through the early work of Stock and Montgomery (1999). The latter forward-modelled river
370 palaeo-profiles, constrained by bedrock strath terraces and basaltic layers, to presently observed
371 profiles for a range of locations worldwide. Their values of *K* range from 10^{-2} to 10^{-4} $m^{0.2}$ yr^{-1} in the
372 mudstones of humid continental Japan, to 10^{-6} - 10^{-7} $m^{0.2}$ yr^{-1} in the subtropical granite landscape of
373 Australia (Stock and Montgomery, 1999). An issue with the experimental approach by Sklar and
374 Dietrich (2001) is that it does not include the effects of weathering and jointing of rock in natural

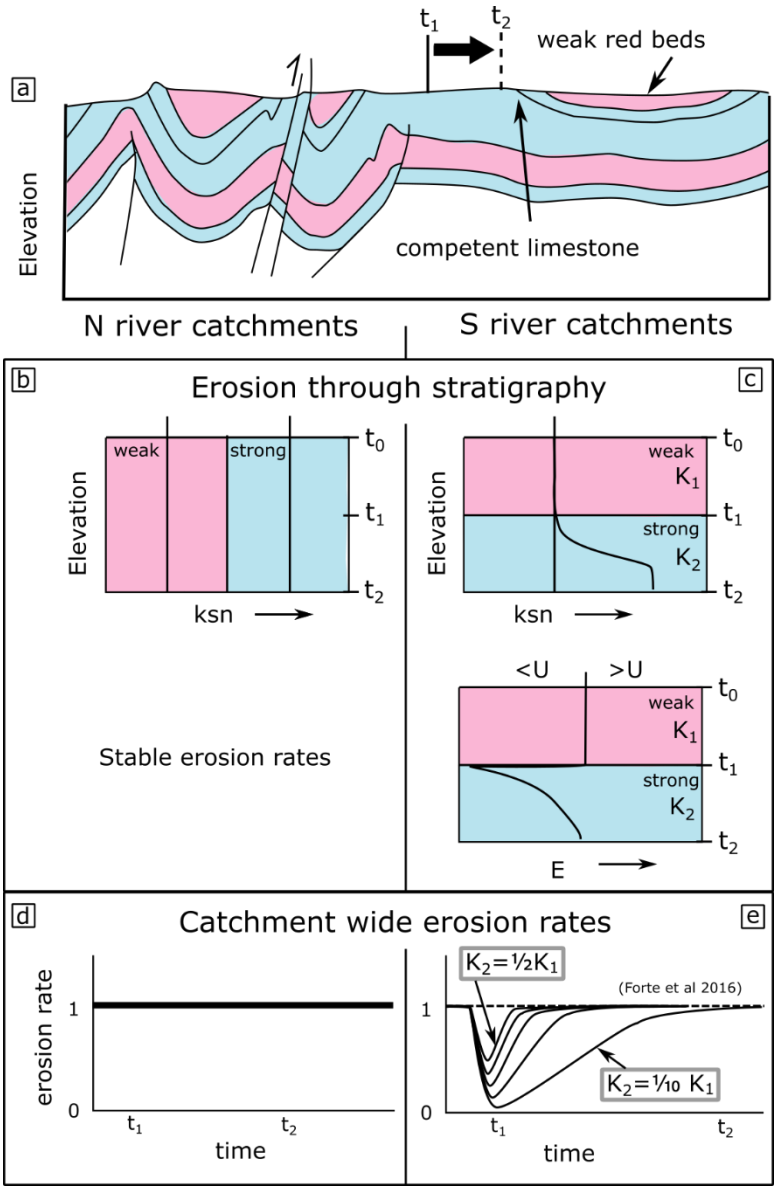

Figure 6: The erosion and exposure of a hard limestone layer underneath a soft red bed layer in the Mesozoic low amplitude syncline (a) leads to a divide mobility towards the southern catchment (Fig. 5). (b) This is because the k_{sn} of the surface exposed needs to adjust to the new lithological strength, steepening transiently as it incises into harder limestone bedrock. (c) The graph for the southern catchments shows the results from landscape evolution modelling of the exposure of a contact between sub-horizontal soft stratigraphy on top of a hard layer (Forte et al., 2016). The resultant change in erosion rates across the divide explains the migration of the drainage divide. The response depends on the factor of difference in erodibility, K, between units.

375 landscapes and their influence on fluvial erodibility. In the results from Stock and Montgomery
376 (1999) the influence of rock-type is difficult to isolate from the variation in climatic setting owing to
377 the spread of study locations. Thus, whilst these early studies give some first order estimates of
378 possible absolute values of fluvial erodibility and the relationship between rock strength and erosion

379 rates, our results constrain more fully the contrasts in fluvial erodibility between rock types which
380 may be expected within one mountain belt.

381 *5.2 Drainage reorganisation in sedimentary cover*

382 The Gilbert metrics indicate drainage divide mobility where it crosses the sedimentary cover in the
383 east (Fig. 5d). Here, the Mesozoic sedimentary cover is gently deformed, resulting in gently dipping
384 strata punctuated by widely spaced thrusts and folds (Fig 1b, Fig 2a). For example, the Dades river
385 catchment south of the main drainage divide (Fig. 6a) incises into a long-wavelength syncline of
386 slightly dipping strata composed of weak continental red beds and hard limestones, whereas directly
387 north of the divide folding and thrusting is more closely spaced resulting in strata dipping at higher
388 angles to the surface (Fig. 6a). Our results show that k_{sn} is correlated to rock strength (Fig. 4e), and in
389 the hard limestone k_{sn} is higher than in the weak red beds (Fig. 4b-c). Whereas erosion through near-
390 vertical strata north of the divide result in near-stable k_{sn} values through time (Fig. 6b), the
391 horizontal stratigraphy of the Dades river catchment to the south of the divide means k_{sn} values
392 need to change through time to return to stable erosion rates (Fig. 6c) which equal uplift rates.
393 Consequently there is a period of transience when k_{sn} values adjust to the change in bedrock
394 erodibility that occurred when erosion of soft red beds exposed hard limestone along the majority of
395 the river catchment (Fig. 1a, 6a). This transition period explains the southwards movement of the
396 divide (Fig. 5d), as erosion rates stay more or less stable in the north (Fig. 6d) whilst transient k_{sn}
397 value causes a temporary decrease in erosion rates in the southern river catchments (Fig. 6e). The
398 stratigraphic effect on river erosion rates presented in Fig. 6e was first demonstrated in a numerical
399 modelling study of river erosion through layered stratigraphy by Forte et al. (2016), who show that
400 for strata of variable erodibility dipping 5° or less the overall erosion rate of the landscape is
401 expected to change by several factors during incision. Here, we show that such an effect can lead to
402 migration of the drainage divide in the gently deformed sedimentary cover in collisional mountain
403 settings, where exhumation of hard and soft strata is isolated or offset by faults.

Simulations by Forte et al. (2016) show the exhumation of a stratigraphic contact with a factor of two to ten difference in erodibility (Fig. 6e) could take 2 - 9 Ma to re-equilibrate in an area of 800 km^2 with a relatively high amount of precipitation (1 m yr^{-1}). Therefore, drainage divide migration in response to the incision through soft red beds to hard limestones in the upper half of the 1500 km^2 Dades catchment, representing a change in erodibility by a factor of 2 - 20 (Fig. 4), where rainfall is on the order of 0.1 - 0.5 m yr^{-1}, is expected to persist on a timescale of 10^6 – 10^7 years.

5.3 Divide migration driven by crystalline basement exhumation

Where crystalline basement is exposed we find the position of the drainage divide is shifting towards the centre of this exposed resistant rock in the High Atlas (Fig. 5). In a numerical simulation, Giachetta et al. (2014) found that when they imposed an erodibility gradient across a drainage divide, which is representative of the exhumation of a crystalline basement, such as in the High Atlas, the drainage divide responded by moving towards the side of lower erodibility over a timescale on the order of 10^6 years. (Bonnet, 2009) proposed that such a shift of the drainage divide is accompanied by a split of catchments, creating more and smaller catchments, on the side of lower erodibility, and Giachetta et al. (2014) show that on the other side, a growth of larger catchments occurs. Similarly, Bernard et al. (2019) found that the drainage divide in the Pyrenees follows the position of strong plutons. This implies that our results show a transient stage of drainage divide migration in response to exhumation of crystalline basement, where today's drainage divide at the edge of the crystalline basement is expected to be stable in the centre of the strong crystalline basement, or might even continue reorganising within the basement to follow the exhumation of resistant plutons. Giachetta et al. (2014) used two orders of magnitude difference in erodibility values to model this effect, and here we show divide mobility can be driven by exhumation of basement that is only a factor of two less erodible than the overlying meta-sedimentary rock if calculated through k_{sn} (Fig. 4d), and a factor of three less erodible if calculated through UCS (Fig. 4c).

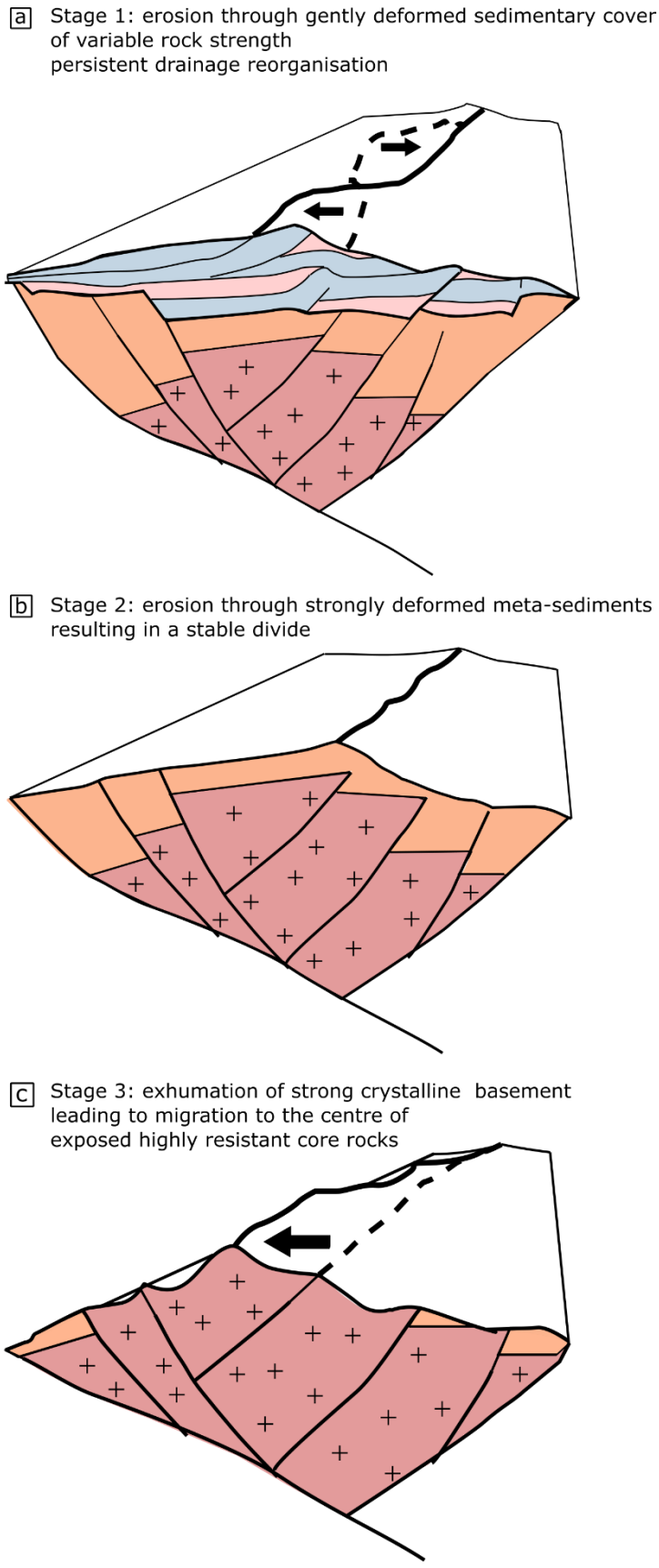

Figure 7 –Conceptual model of the development of a collisional mountain belt and the behaviour of the central drainage divide in response to exhumation of lithostratigraphic units

5.4 Lithologically induced drainage divide mobility during the long term erosion of a collisional mountain belt

The combination of estimations of contrasts in fluvial erodibility of rock types (Fig. 4), geomorphic indicators of drainage mobility (Fig. 5), and considerations of their structural configuration in the High Atlas compared to numerical simulation studies (see sections 5.1 - 5.3) enables us to put forward a model of drainage divide mobility during the erosion of a mountain belt. The overall trend of the drainage divide, strike of faults and bedding planes follows the structural grain of the mountain belt (Fig. 1), for example determined by the pre-existing structure of an extensional rift such as in the High Atlas (Babault et al., 2012). We propose changes in erosion rates as rivers incise through strata of different erodibility will lead to drainage reorganisation in collisional mountain belts, where layers are close to horizontal and only gently deformed (Fig. 6, 7). This is because where strata are deformed gently and offset by faults, local exhumation of contacts between soft and hard rock leads to changes in erosion rates between catchments (Fig. 6). Consequent changes in erosion rates across the drainage divide will lead to the migration of the drainage divide (Fig. 7a) as illustrated by the mobility of the drainage divide in the High Atlas (Fig 5, 6), which could lead to steady divide migration or instantaneous capture of catchments, such as shown in the Appalachians (Gallen, 2018). The effect of rock type on drainage reorganisation will be strongest in early phases of collisional mountain building, before the sedimentary cover erodes in the centre of the belt. In later stages, minor reorganisation and capture could still occur closer to the thrust front on the margins of the mountain belt where Mesozoic sedimentary strata are present. When deformed meta-sediments become exhumed, the increase in dip and deformation of strata leads to more stable erosion as rivers incise (Forte et al., 2016, Fig. 6), resulting in stable drainage divides as witnessed in the middle of the study area (Fig 5, 7b). When crystalline basement gets exhumed, the drainage divide will migrate into the centre of highly resistant rocks resulting in more drainage divide migration (Fig 5, 7). The migration of the main drainage divide in a mountain belt has been shown to lead to reorganisation of river catchments (Bonnet, 2009; Giachetta et al., 2014), imposing new boundary

conditions on river channels which change gradients and sediment loads (Forte et al., 2015) and the ensuing response can result in a cascading effect, impacting geomorphic and stratigraphic systems for millions to tens of millions of years (Beeson et al., 2017).

Conclusions

This study shows that in a collisional mountain belt, the drainage divide will be mobile in response to changes in erosion rates of rivers incising into gently dipping and deformed strata of contrasting erodibility in the sedimentary cover, and in response to the exhumation of strong crystalline basement. A combination of rock mass strength measurements and k_{sn} derived from a digital elevation model constrain the contrasts in fluvial erodibility exhibited in the High Atlas to between a factor of 4 calculated through k_{sn} and two orders of magnitude calculated through UCS. In the stage of a collisional mountain belt during which rivers incise through highly deformed meta-sedimentary units of intermediate erodibility, rock-type induced boundary conditions affect river networks the least. Based on our values of erodibility contrast and previous numerical models we estimate the timescale of adjustment in response to changes in erodibility of exposed bedrock to be on the order of 10^6-10^7 years. Our results demonstrate that the mobility of the drainage divide in a collisional mountain belt can be driven by rock erodibility variation alone, which has implications for the perception of autogenic dynamism of drainage networks and fluvial erosion in collisional mountain belts, and the interpretation of their geomorphology and downstream stratigraphy.

Author contributions

J.R.Z. drafted the article with critical revision and intellectual input from co-authors according to the following contribution: M.S., S.J.B., M.T., A.E.M.. J.R.Z., M.S., A.E.M. and S.J.B. performed the Schmidt hammer measurements in the field, J.R.Z. performed the topographic analysis. J.R.Z., M.S. and S.J.B. initiated the project.

Funding

Fieldwork to validate topographic analysis and take Schmidt hammer measurements during J.R.Z.'s PhD was supported by a University of Plymouth PhD studentship and the Geological Remote Sensing Group Student Award.

References cited (50 refs)

Allen, G.H., Barnes, J.B., Pavelsky, T.M., Kirby, E., 2013. Lithologic and tectonic controls on bedrock channel form at the northwest Himalayan front. Journal of Geophysical Research: Earth Surface 118, 1806-1825.

Anton, L., Mather, A.E., Stokes, M., Muñoz-Martin, A., De Vicente, G., 2015. Exceptional river gorge formation from unexceptional floods. Nature Communications 6, 7963.

Babault, J., Teixell, A., Arboleya, M.L., Charroud, M., 2008. A Late Cenozoic age for long-wavelength surface uplift of the Atlas Mountains of Morocco. Terra Nova 20, 102-107.

Babault, J., Van Den Driessche, J., Teixell, A., 2012. Longitudinal to transverse drainage network evolution in the High Atlas (Morocco): The role of tectonics. Tectonics 31, n/a-n/a.

Baynes, E.R.C., Attal, M., Niedermann, S., Kirstein, L.A., Dugmore, A.J., Naylor, M., 2015. Erosion during extreme flood events dominates Holocene canyon evolution in northeast Iceland. Proceedings of the National Academy of Sciences 112, 2355-2360.

Beeson, H.W., McCoy, S.W., Keen-Zebert, A., 2017. Geometric disequilibrium of river basins produces long-lived transient landscapes. Earth and Planetary Science Letters 475, 34-43.

Bernard, T., Sinclair, H.D., Gailleton, B., Mudd, S.M., Ford, M., 2019. Lithological control on the post-orogenic topography and erosion history of the Pyrenees. Earth and Planetary Science Letters 518, 53-66.

Bonnet, S., 2009. Shrinking and splitting of drainage basins in orogenic landscapes from the migration of the main drainage divide. Nature Geoscience 2, 766.

Boulton, S.J., Stokes, M., 2018. Which DEM is best for analyzing fluvial landscape development in mountainous terrains? Geomorphology 310, 168-187.

Boulton, S.J., Stokes, M., Mather, A.E., 2014. Transient fluvial incision as an indicator of active faulting and Plio-Quaternary uplift of the Moroccan High Atlas. Tectonophysics 633, 16-33.

Brocard, G.Y., van der Beek, P.A., 2006. Influence of incision rate, rock strength, and bedload supply on bedrock river gradients and valley-flat widths: Field-based evidence and calibrations from western Alpine rivers (southeast France). 398, 101-126.

Bursztyn, N., Pederson, J.L., Tressler, C., Mackley, R.D., Mitchell, K.J., 2015. Rock strength along a fluvial transect of the Colorado Plateau – quantifying a fundamental control on geomorphology. Earth and Planetary Science Letters 429, 90-100.

Errarhaoui, K., 1998. Structure du haut-atlas : plis et chevauchements du socle et de couverture (interpretations des donnees geophysiques et geologiques), p. 326 P.

Fick, S.E., Hijmans, R.J., 2017. WorldClim 2: new 1-km spatial resolution climate surfaces for global land areas. International Journal of Climatology 37, 4302-4315.

Forte, A.M., Whipple, K.X., 2018. Criteria and tools for determining drainage divide stability. Earth and Planetary Science Letters 493, 102-117.

Forte, A.M., Whipple, K.X., 2019. Short communication: The Topographic Analysis Kit (TAK) for TopoToolbox. Earth Surf. Dynam. 7, 87-95.

Forte, A.M., Whipple, K.X., Cowgill, E., 2015. Drainage network reveals patterns and history of active deformation in the eastern Greater Caucasus. Geosphere 11, 1343-1364.

Forte, A.M., Yanites, B.J., Whipple, K.X., 2016. Complexities of landscape evolution during incision through layered stratigraphy with contrasts in rock strength. Earth Surface Processes and Landforms 41, 1736-1757.
Gallen, S.F., 2018. Lithologic controls on landscape dynamics and aquatic species evolution in post-orogenic mountains. Earth and Planetary Science Letters 493, 150-160.
Giachetta, E., Refice, A., Capolongo, D., Gasparini, N.M., Pazzaglia, F.J., 2014. Orogen-scale drainage network evolution and response to erodibility changes: insights from numerical experiments. Earth Surface Processes and Landforms 39, 1259-1268.
Gilbert, G.K., 1877. Report on the Geology of the Henry Mountains. US Government Printing Office.
Gokceoglu, C., Aksoy, H., 2000. New approaches to the characterization of clay-bearing, densely jointed and weak rock masses. Engineering Geology 58, 1-23.
Goktan, R.M., Gunes, N., 2005. Technical note. International Journal of Rock Mechanics and Mining Sciences 42, 466-472.
Goudie, A.S., 2006. The Schmidt Hammer in geomorphological research. Progress in Physical Geography: Earth and Environment 30, 703-718.
He, C., Rao, G., Yang, R., Hu, J., Yao, Q., Yang, C.-J., 2019. Divide migration in response to asymmetric uplift: Insights from the Wula Shan horst, North China. Geomorphology 339, 44-57.
Howard, A.D., Dietrich, W.E., Seidl, M.A., 1994. Modeling fluvial erosion on regional to continental scales. Journal of Geophysical Research: Solid Earth 99, 13971-13986.
Hughes, P.D., Gibbard, P.L., Woodward, J.C., 2004. Quaternary glaciation in the Atlas Mountains of North Africa, in: Ehlers, J., Gibbard, P.L. (Eds.), Developments in Quaternary Sciences. Elsevier, pp. 255-260.
Kahraman, S., Fener, M., Gunaydin, O., 2002. Predicting the Schmidt hammer values of in-situ intact rock from core sample values. International Journal of Rock Mechanics and Mining Sciences 39, 395-399.
Kahraman, S., Fener, M., Kozman, E., 2012. Predicting the compressive and tensile strength of rocks from indentation hardness index. Journal of the Southern African Institute of Mining and Metallurgy 112, 331-339.
Karakus, M., Kumral, M., Kilic, O., 2005. Technical note. International Journal of Rock Mechanics and Mining Sciences 42, 323-330.
Katz, O., Reches, Z., Roegiers, J.-C., 2000. Evaluation of mechanical rock properties using a Schmidt Hammer. International Journal of rock mechanics and mining sciences 37, 723-728.
Mather, A.E., Stokes, M., 2018. Bedrock structural control on catchment-scale connectivity and alluvial fan processes, High Atlas Mountains, Morocco. Geological Society, London, Special Publications 440, 103-128.
Mudd, S.M., Attal, M., Milodowski, D.T., Grieve, S.W.D., Valters, D.A., 2014. A statistical framework to quantify spatial variation in channel gradients using the integral method of channel profile analysis. Journal of Geophysical Research: Earth Surface 119, 138-152.
Nazir, R., Momeni, E., Armaghani, D.J., Amin, M.M., 2013. Correlation between unconfined compressive strength and indirect tensile strength of limestone rock samples. Electronic Journal of Geotechnical Engineering 18, 1737-1746.
Pastor, À., Teixell, A., Arboleya, M.L., 2012. Rates of Quaternary deformation in the Ouarzazate Basin (Southern Atlas Front, Morocco). 2013 55.
Perne, M., Covington, M.D., Thaler, E.A., Myre, J.M., 2017. Steady state, erosional continuity, and the topography of landscapes developed in layered rocks. Earth Surf. Dynam. 5, 85-100.
Pye, K., Goudie, A.S., Watson, A., 1986. Petrological influence on differential weathering and inselberg development in the Kora area of central Kenya. Earth Surface Processes and Landforms 11, 41-52.
Roy, S.G., Koons, P.O., Upton, P., Tucker, G.E., 2015. The influence of crustal strength fields on the patterns and rates of fluvial incision. Journal of Geophysical Research: Earth Surface 120, 275-299.

Saadi, M., Hilali, E.A., Bensaid, M., Boudda, A., Dahmani, M., 1985. Carte Géologique du Maroc Notes et mémoires (Morocco. Service Géologique). Editions du Service Géologique du Maroc.
Schanz, S.A., Montgomery, D.R., 2016. Lithologic controls on valley width and strath terrace formation. Geomorphology 258, 58-68.
Sklar, L.S., Dietrich, W.E., 2001. Sediment and rock strength controls on river incision into bedrock. Geology 29, 1087-1090.
Stock, J.D., Montgomery, D.R., 1999. Geologic constraints on bedrock river incision using the stream power law. Journal of Geophysical Research. B 104, 4983-4993.
Stokes, M., Mather, A.E., Belfoul, A., Farik, F., 2008. Active and passive tectonic controls for transverse drainage and river gorge development in a collisional mountain belt (Dades Gorges, High Atlas Mountains, Morocco). Geomorphology 102, 2-20.
Stokes, M., Mather, A.E., Belfoul, M., Faik, F., Bouzid, S., Geach, M.R., Cunha, P.P., Boulton, S.J., Thiel, C., 2017. Controls on dryland mountain landscape development along the NW Saharan desert margin: Insights from Quaternary river terrace sequences (Dadès River, south-central High Atlas, Morocco). Quaternary Science Reviews 166, 363-379.
Teixell, A., Arboleya, M.-L., Julivert, M., Charroud, M., 2003. Tectonic shortening and topography in the central High Atlas (Morocco). Tectonics 22, n/a-n/a.
Wang, Y., Wang, P., Ge, W., Zhou, R., Schoenbohm, L.M., Zhang, B., Zhang, J., Yuan, Z., Li, X., 2019. Differential crustal deformation across the Cona-Oiga rift, southern Tibetan Plateau. Journal of Asian Earth Sciences 177, 177-185.
Whipple, K.X., Forte, A.M., DiBiase, R.A., Gasparini, N.M., Ouimet, W.B., 2017. Timescales of landscape response to divide migration and drainage capture: Implications for the role of divide mobility in landscape evolution. Journal of Geophysical Research: Earth Surface 122, 248-273.
Whipple, K.X., Tucker, G.E., 1999. Dynamics of the stream-power river incision model: Implications for height limits of mountain ranges, landscape response timescales, and research needs. Journal of Geophysical Research: Solid Earth 104, 17661-17674.
Willett, S.D., McCoy, S.W., Perron, J.T., Goren, L., Chen, C.-Y., 2014. Dynamic Reorganization of River Basins. Science 343.
Wobus, C., Whipple, K.X., Kirby, E., Snyder, N., Johnson, J., Spyropolou, K., Crosby, B., Sheehan, D., 2006. Tectonics from topography: Procedures, promise, and pitfalls. Geological Society of America Special Papers 398, 55-74.
Yanites, B.J., Becker, J.K., Madritsch, H., Schnellmann, M., Ehlers, T.A., 2017. Lithologic Effects on Landscape Response to Base Level Changes: A Modeling Study in the Context of the Eastern Jura Mountains, Switzerland. Journal of Geophysical Research: Earth Surface 122, 2196-2222.